Marine Chemistry 218 (2020) 103733

Contents lists available at ScienceDirect

Marine Chemistry

journal homepage: www.elsevier.com/locate/marchem

Character and sedimentation of "lingering" Macondo oil to the deep-sea after the Deepwater Horizon oil spill

Uta Passow[a,b,*], Scott A. Stout[c]

[a] Memorial University of Newfoundland, Canada
[b] University of California Santa Barbara, CA, United States
[c] NewFields Environmental Forensics Practice, LLC, Rockland, MA, United States

ARTICLE INFO

Keywords:
Deepwater Horizon
Oil sedimentation
Macondo oil weathering
Gulf of Mexico

ABSTRACT

During the active 87-day *Deepwater Horizon* spill in the northern Gulf of Mexico, a significant fraction of the spilled Macondo oil was transported to the seafloor via the sedimentation of marine snow. Here we present a detailed characterization of oil that arrived together with marine snow at a 1400 m deep sediment trap six weeks to 13 months after the spill had ended. These data give insight into the nature and evolution of the sedimentation of the marine snow and oil, the latter of which remained as droplets in the water column after the spill ended. Four pulses of oil flux were recognized; three of which were associated with peak sedimentation rates of diatoms. Detailed chemical analysis (TPH, alkylated PAH, and petroleum biomarker fingerprints) reveal the sinking oil's lack of evaporation and photo-oxidation, which indicated it was not derived from the sea surface but had "lingered" within the water column after the spill. Measurable amounts of the increasingly weathered (biodegraded and water-washed) Macondo oil was collected in the trap for ~1 year after the active spill ended, over which time the oil flux decreased overall. The results indicate that sinking diatom aggregates and other marine snow scavenged measurable amounts of weathered Macondo oil droplets remaining in the water, and carried them to the deep-seafloor for approximately 1-year after the spill ended.

1. Introduction

The *Deepwater Horizon* (DwH) accident in April 2010 in the Gulf of Mexico, resulted in the continuous release of large amounts of crude oil and gas at a water depth of about 1500 m until the leak could be sealed 87 days later, in mid-July 2010. Whereas a large fraction of the spilled oil reached the sea surface forming slicks, mousses, and sheens at the water-atmosphere interface, another significant portion remained physically or chemically-dispersed and dissolved in the water column, with a large fraction forming a deep-sea intrusion layer, or "plume", characterized by elevated concentrations of hydrocarbons at ~1000 to 1300 m depth (Camilli et al., 2010; Socolofsky et al., 2011). Deep water column studies tracked the plume in multiple directions (Boehm et al., 2016; Spier et al., 2013), but mostly toward the southwest where oil droplets were still recognized ~155 km from the well (Payne and Driskell, 2018). Monitoring of the water column southwest of the well after the spill ended continued to detect "lingering" oil, as evidenced by trace concentrations (0.001 to 0.1 μg/L) of total (50) polycyclic aromatic hydrocarbons (PAHs), in most of the approximately 1300 samples collected in August to December 2010 (Boehm et al., 2016).

Numerous sediment studies have shown that some fraction of the spilled oil, estimated between 2 and 20% of the oil released, was deposited over large areas of the seafloor (Brooks et al., 2015; Chanton et al., 2015; Passow and Ziervogel, 2016; Romero et al., 2015, 2017; Stout and Payne, 2016a; Stout et al., 2016a, 2017; Valentine et al., 2014) where it impacted benthic organisms and ecosystems (e.g. Fisher et al., 2014, 2016; Montagna et al., 2013; Murawski et al., 2014; Schwing et al., 2018).

The mechanisms by which oil reached the seafloor during the DwH spill included direct impingement of the deep-sea plume onto topographic features within the deep-sea plume's path, but this mechanism alone cannot explain the widespread "footprint" of seafloor impact recognized – which extended to shelf sediments that lay above the depth of the deep-sea plume (Brooks et al., 2015; Stout and German, 2018). Close to the failed Macondo well, sedimentation of oil-particle-aggregates (OPAs) (Gong et al., 2014; Lee, 2002) consisting predominantly of oil associated with synthetic-based drilling mud (SBM), resulted in a 6.5 km^2 "footprint" around the well up to 10 cm thick (Stout and Payne, 2017). This drilling mud was discharged during the initial DwH blowout, the rig's sinking, and (mostly) the failed top-kill

* Corresponding author at: Memorial University of Newfoundland, Canada.
E-mail address: uta.passow@mun.ca (U. Passow).

https://doi.org/10.1016/j.marchem.2019.103733

Available online 29 November 2019

response operations. Further removed from the well, and after the leak was closed, sinking marine snow is considered the dominant mechanism by which oil reached the seafloor (Brooks et al., 2015; Daly et al., 2016; Hastings et al., 2014; Hastings et al., 2016; Larson et al., 2018; Passow and Ziervogel, 2016; Quigg et al., 2019; Romero et al., 2015, 2017; Schwing et al., 2017; Valentine et al., 2014; Yan et al., 2016).

Marine snow, defined as composite particles > 0.5 mm, is not uniquely formed during oil spills. It forms due to zooplankton activities, e.g. from feeding structures (Alldredge and Silver, 1988), due to physical coagulation of smaller particles, like algae, detritus or feces (Jackson, 2005), or, in the presence of oil, due to bacterial activity. Diatoms, specifically, are known to regularly cause large sedimentation events, as coagulation of cells at bloom termination is part of their lifecycle (Smetacek, 1985). Such mass sedimentation episodes of diatom aggregates have long been known to capture suspended or slowly sinking particles, such as clay or plastic, carrying them downward, literally cleaning the water column of such material (Kumar et al., 1998; Long et al., 2015; Passow, 2004; Passow et al., 2001). A similar scavenging mechanisms was found to occur for dispersed oil droplets, and was likely of importance both, during and after the DwH spill (Passow, 2016; Passow et al., 2019; 2017; Wirth et al., 2018). In contrast to marine snow, bacterial agglomerations appear to be a direct response to the presence of oil, where oil degrading bacteria form a biofilm that coats oil droplets in the water column or surface slicks and leads to mucus rich particles (Baelum et al., 2012; Doyle et al., 2018; Hazen et al., 2010; Passow, 2016; Passow et al., 2012; Ziervogel et al., 2012). Such microbial agglomerations, which especially at the sea surface may reach marine snow size, likely were a significant transport vehicle for oil or weathered oil only as long as concentrations of oil in the water were relatively high, e.g. during the active spill.

Sedimentation dynamics can be studied with moored sediment traps deployed above the seafloor. Such traps collect and preserve sinking material in situ, with each sample integrating over 2–4 week intervals, thereby allowing for its study to be isolated from any seafloor influences, such as mixing with "background" hydrocarbons, bioturbation, degradation and resuspension. Unfortunately, sediment trap studies during oil spill events are limited with respect to their location and/or the time of deployment relative to a spill. During the active DwH spill, a sediment trap deployed along the shelf edge (400-450 m water depth) 58 km northeast of the failed Macondo well, demonstrated oil fluxes were 19- to 44-times higher during the active spill than pre- and post-spill background values (Stout and German, 2018).

Another sediment trap deployed in late August/ early September 2010, provided the opportunity to assess the sinking of any oil that may have occurred about 6 weeks to 13 months *after* the DwH spill ended on July 15 (Yan et al., 2016). This trap was located in the deep-sea (~1400 m water depth; 100 m above the seafloor) and ~6.5 km southwest of the failed Macondo well, and collected 20 trap samples at 21-day intervals, each (Fig. 1). Although visually no oil was present 6 weeks after the spill, trap samples, especially those collected during the remainder of 2010, contained significant amounts of oil-derived compounds, as well as indicators of SBM (olefins) and combustion products (Yan et al., 2016). Results showed that near the spill site four distinct sedimentation pulses continued to carry oil to the deep seafloor in the months following the end of the DwH spill. Three of these pulses were dominated by diatom blooms, which indicates that sedimentation of diatom aggregates specifically, continued to transport "lingering" oil to the seafloor after the DwH ended. Likely, bacterial agglomerations that contributed to the sedimentation of oil during the spill, when oil concentrations where high, played no role for the sedimentation of oil after the spill.

In the present study, the detailed composition of "lingering" oil that sank to 1400 m approximately 6.5 km southwest of the Macondo well in the year after the spill is reported (Fig. 1). First, we briefly discuss the temporal sequence of total and specific hydrocarbon fluxes and their

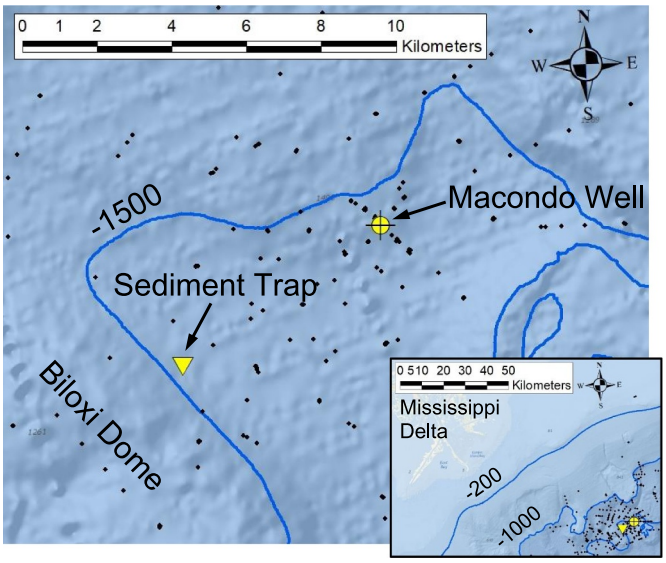

Fig. 1. Map showing the location of the sediment trap relative to the Macondo well. Inset shows locations relative to Mississippi Delta. Bathymetric contours (m) and locations of 728 sediment cores analyzed as part of the NRDA investigation (Stout et al., 2016a; black dots) are indicated. Yan et al. (2016) analyzed samples from this same sediment trap.

association with the sedimentation of marine snow. Then, the detailed chemical characteristics of the oil, i.e., their chemical fingerprints, are presented, which informs on both the origin of the oil and its weathering over time. The specific types of oil-derived compounds that are shown to arrive at the seafloor (e.g., polycyclic aromatic hydrocarbons; PAHs) may also help in identifying potential threats to benthic organisms and ecosystems months after an oil spill as the water column progressively recovers.

2. Methods

2.1. Sample collection

Sedimentation rates of mass (dry weight), biogenic silica (BSi), particulate organic carbon (POC) and nitrogen (PON) as well as flux of hydrocarbons were measured using a sediment trap (KUM) that was deployed at 28° 42.360′N; 88° 25.325′W, approximately 6.5 km (4 mi) southwest of the Macondo well and 1.6 km east of Biloxi Dome (Fig. 1). The water depth at this location was 1538 m and the trap was deployed about 105 m above the seafloor. A detailed analysis of oil compounds associated with the sinking material was conducted (Section 2.4).

Sample bottles (300 mL polypropylene) on a carousel below the funnel-shaped trap (collection surface 0.5 m^2) collected 20 samples over 21-day intervals starting August 25, 2010 and ending September 28, 2011 (Table 1; Cup 20 collected Sept. 29-Oct. 19, 2011 contained insufficient material for study). Bottle contents were preserved in situ during collection with $HgCl_2$ and upon retrieval were maintained cold (4 °C) and dark until processed for analysis. Collected material was split repeatedly using a Folsom Plankton splitter and whole splits or fractions of splits were used for the analysis. See Yan and co-authors for details (Yan et al., 2016).

2.2. Particle flux rates

Appropriate fractions of 1/128th split were used for the analysis of mass flux rate (dry weight, DW), particulate organic carbon (POC), particulate organic nitrogen (PON), and biogenic silica flux (BSi). Quadruplicate samples were filtered onto pre-weighed (AE160, Mettler Toledo) and pre-combusted (450 °C for 4–6 h) GF/F filters (25 mm

Table 1
Inventory of sediment trap material (material collected in cup 20, the last cup, was not sufficient for analysis) DW = dry weight

Cup #	Sample ID	Open Date	Close Date	Fraction of total sample	Total Mass (g DW cup^{-1})
1	GoM2010-2011_S1_C1_1-16	25-Aug-10	15-Sep-10	1/16	19.3
2	GoM2010-2011_S1_C2_1-8	15-Sep-10	6-Oct-10	1/8	7.1
3	GoM2010-2011_S1_C3_1-8	6-Oct-10	27-Oct-10	1/8	5.6
4	GoM2010-2011_S1_C4_1-8	27-Oct-10	17-Nov-10	1/8	5.8
5	GoM2010-2011_S1_C5_1-8	17-Nov-10	8-Dec-10	1/8	2.8
6	GoM2010-2011_S1_C6_1-8	8-Dec-10	29-Dec-10	1/8	6.5
7	GoM2010-2011_S1_C7_1-8	29-Dec-10	19-Jan-11	1/8	5.4
8	GoM2010-2011_S1_C8_1-8	19-Jan-11	9-Feb-11	1/8	4.4
9	GoM2010-2011_S1_C9_1-8	9-Feb-11	2-Mar-11	1/8	5.1
10	GoM2010-2011_S1_C10_1-8	2-Mar-11	23-Mar-11	1/8	16.1
11	GoM2010-2011_S1_C11_1-8	23-Mar-11	13-Apr-11	1/8	8.3
12	GoM2010-2011_S1_C12_1-8	13-Apr-11	4-May-11	1/8	8.3
13	GoM2010-2011_S1_C13_1-8	4-May-11	25-May-11	1/8	4.2
14	GoM2010-2011_S1_C14_1-8	25-May-11	15-Jun-11	1/8	5.7
15	GoM2010-2011_S1_C15_1-8	15-Jun-11	6-Jul-11	1/8	5.1
16	GoM2010-2011_S1_C16_1-8	6-Jul-11	27-Jul-11	1/8	4.1
17	GoM2010-2011_S1_C17_1-8	27-Jul-11	17-Aug-11	1/8	4.1
18	GoM2010-2011_S1_C18_1-8	17-Aug-11	7-Sep-11	1/8	4.8
19	GoM2010-2011_S1_C19_1-8	7-Sep-11	28-Sep-11	1/16	3.5

diameter, nominal poresize 0.7 μm, Whatman), briefly rinsed with Milli-Q water, dried at 60 °C (4–6 h), and weighed. DW was defined as the difference between dried and pre-weighed filters. Total mass flux rate (dry weight flux) was calculated from the filtered volume of the split, the split size, collection area and collection time of the trap cup. The total dry weight of material collected in each sample cup ranged from 19.3 g (Cup 1) to 2.8 g (Cup 5; Table 1) and quadruplicates varied by < 6%.

Duplicate filters were then used to determine particular organic carbon (POC) and particulate organic nitrogen (PON) using a CHN elemental analyzer (CEC 44OHA; Control Equipment, now Exeter Analytical). Biogenic silica (BSi) was analyzed by filtering splits onto 0.6-μm polycarbonate filters (47 mm diameter, Millipore) (DeMaster, 1981; Mortlock and Froelich, 1989). Filters were hydrolyzed with Na_2CO_3 running a 0.5 to 5 h-time series and analyzed colorimetrically (Shipe and Brzezinski, 2001). The change in the slope of dissolution rate indicates the shift from $bSiO_2$ to lithogenic silica dissolution and was used to determine BSi concentration. BSi was assumed to have a molar mass of 67. Select samples were investigated microscopically and recognizable particles such as diatom frustules and fecal pellets enumerated. Particles were counted on phase contrast using an inverted microscope (IM 35, Zeis) according to the Utermöhl method (Utermöhl, 1958). Only dominant, identifiable frustules, cells and pellets were considered. Total flux rate (mg m^{-2} d^{-1}) of all particulates (DW, POC/PON, BSi, diatoms, feces) was calculated based on the trap surface area (0.5 m^2), deployment time of each jar, split size, and subsample volume and measured concentration.

2.3. Hydrocarbon flux

Flux rate of total petroleum hydrocarbons (TPH), selected PAH totals (TPAH16 and TPAH50; defined below), 17α(H),21β(H)-hopane (hopane) and perylene were determined. Splits (1/8th or 1/16th, Table 1) of the total particulates collected in each bottle were provided to Alpha Analytical Laboratory (Mansfield, MA), where they were transferred to pre-weighed 250 mL glass extraction jars and centrifuged in order to concentrate the collected material. The concentrated material was split with an aliquot used for a separate dry weight determination used only to report hydrocarbon concentrations and the remainder was used for chemical analysis (Section 2.4). Flux rates for TPH, TPAH16, TPAH50, and hopane were calculated by multiplying the concentration of these hydrocarbons in trap samples (μg/g dry) by the total dry weight of particles in the trap samples (g dry; Table 1) divided by 0.5 m^2 (surface area of the trap) then divided by the days deployed (days).

2.4. Sample extraction and analysis

Splits (1/8th or 1/16th; Table 1) from each cup sample were analyzed for various hydrocarbons commonly used in the assessment of oil in the environment. The samples were spiked with recovery internal surrogates (RIS; 5α-androstane, acenaphthene-d10, chrysene-d12) and serially-extracted (3×) using fresh dichloromethane (DCM). Each sample's serial extracts were combined, dried with sodium sulfate, and concentrated to 1 mL using Kuderna Danish apparatus and nitrogen blow-down. The concentrated extracts were then processed through silica gel, eluting with DCM, following adaptations of EPA Method 3630 and re-concentrated to 1 mL (as above). The concentrated silica-cleaned extracts were then spiked with surrogate internal standards (SIS; *o*-terphenyl, n-tetracosane-d50, 2-methylnaphthalene-d10, pyrene-d10, benzo(b)fluoranthene-d12, and 5β(H)-cholane) prior to instrument analysis.

All sample extracts were analyzed using (1) modified EPA Method 8015B and (2) modified EPA Method 8270 as described in the following paragraphs. Additional details of these methods are described elsewhere (Douglas et al. 2015). A modified EPA Method 8015B was used to determine the total petroleum hydrocarbon (TPH) concentration (C_9-C_{44}) and concentrations of individual *n*-alkanes (C_9-C_{40}) and (C_{15}-C_{20}) acyclic isoprenoids via gas chromatography-flame ionization detection (GC/FID). This analysis also provided a high resolution “chemical fingerprint” of the oil contained within the trap samples. Additionally, the concentrations of (1) 60 PAH, alkylated PAH homologues, decalins, and sulfur-containing aromatics and (2) 54 tricyclic and pentacyclic triterpanes (including 17α(H),21β(H)-hopane; hopane), regular and rearranged steranes, and triaromatic steroids was determined via gas chromatography–mass spectrometry (GC/MS) operated in the selected ion monitoring mode (SIM; modified EPA Method 8270). In addition to measuring the concentrations of PAHs and biomarkers in the trap samples, this analysis provided “chemical fingerprints” that were compared to fresh and weathered Macondo oil (studied previously; see below). A complete list of these PAH and petroleum biomarker analytes is given in Table 2. Note that two PAH totals are discussed herein, viz. TPAH16 and TPAH50 (Table 2). TPAH16 represents the total of 16 Priority Pollutant PAH analytes and TPAH50 represents the total of all 2- to 6-ring PAH analytes ranging from naphthalene to benzo(*g,h,i*) perylene, excluding perylene.

The TPH, SHC, PAH and biomarker concentrations are non-surrogate corrected and are reported on a dry weight basis (μg/g dry). Concentrations of all individual analytes in the samples are provided in the Supporting Information.

Table 2
Inventory and abbreviations of target analytes for the PAH and petroleum biomarkers quantified.

PAH and related analytes	
Abbrev	Analytes
D0	cis/trans-Decalin
D1	C1-Decalins
D2	C2-Decalins
D3	C3-Decalins
D4	C4-Decalins
BT0	Benzothiophene
BT1	C1-Benzo(b)thiophenes
BT2	C2-Benzo(b)thiophenes
BT3	C3-Benzo(b)thiophenes
BT4	C4-Benzo(b)thiophenes
N0	**Naphthalene**
N1	C1-Naphthalenes
N2	C2-Naphthalenes
N3	C3-Naphthalenes
N4	C4-Naphthalenes
B	Biphenyl
DF	Dibenzofuran
AY	**Acenaphthylene**
AE	**Acenaphthene**
F0	**Fluorene**
F1	C1-Fluorenes
F2	C2-Fluorenes
F3	C3-Fluorenes
A0	**Anthracene**
P0	**Phenanthrene**
PA1	C1-Phenanthrenes/Anthracenes
PA2	C2-Phenanthrenes/Anthracenes
PA3	C3-Phenanthrenes/Anthracenes
PA4	C4-Phenanthrenes/Anthracenes
DBT0	Dibenzothiophene
DBT1	C1-Dibenzothiophenes
DBT2	C2-Dibenzothiophenes
DBT3	C3-Dibenzothiophenes
DBT4	C4-Dibenzothiophenes
BF	Benzo(b)fluorene
FL0	**Fluoranthene**
PY0	**Pyrene**
FP1	C1-Fluoranthenes/Pyrenes
FP2	C2-Fluoranthenes/Pyrenes
FP3	C3-Fluoranthenes/Pyrenes
FP4	C4-Fluoranthenes/Pyrenes
NBT0	Naphthobenzothiophenes
NBT1	C1-Naphthobenzothiophenes
NBT2	C2-Naphthobenzothiophenes
NBT3	C3-Naphthobenzothiophenes
NBT4	C4-Naphthobenzothiophenes
BA0	**Benz [*a*] anthracene**
C0	**Chrysene/Triphenylene**
BC1	C1-Chrysenes
BC2	C2-Chrysenes
BC3	C3-Chrysenes
BC4	C4-Chrysenes
BBF	Benzo[*b*]fluoranthene
BJKF	**Benzo [*jk*] fluoranthene**
BAF	**Benzo [*a*] fluoranthene**
BEP	Benzo[*e*]pyrene
BAP	**Benzo [*a*] pyrene**
PER	Perylene
IND	**Indeno [1,2,3-*cd*] pyrene**
DA	**Dibenz [*a,h*] anthracene**
GHI	**Benzo [*g,h,i*] perylene**
TPAH50	Σ N0 through GHI, excl PER
TPAH16	**Σ bold compounds**

Petroleum biomarker analytes	
Abbrev	Analytes
T4	C23 Tricyclic Terpane
T5	C24 Tricyclic Terpane
T6	C25 Tricyclic Terpane
T6a	C24 Tetracyclic Terpane
T6b	C26 Tricyclic Terpane-22S
T6c	C26 Tricyclic Terpane-22R
T7	C28 Tricyclic Terpane-22S
T8	C28 Tricyclic Terpane-22R
T9	C29 Tricyclic Terpane-22S
T10	C29 Tricyclic Terpane-22R
T11	18a-22,29,30-Trisnorneohopane-TS
T11a	C30 Tricyclic Terpane-22S
T11b	C30 Tricyclic Terpane-22R
T12	17a(H)-22,29,30-Trisnorhopane-TM
T14a	17a/b,21b/a 28,30-Bisnorhopane
T14b	17a(H),21b(H)-25-Norhopane
T15	30-Norhopane
T16	18a(H)-30-Norneohopane-C29Ts
X	17a(H)-Diahopane
T17	30-Normoretane
T18	18a(H)&18b(H)-Oleananes
T19	Hopane
T20	Moretane
T21	30-Homohopane-22S
T22	30-Homohopane-22R
T26	30,31-Bishomohopane-22S
T27	30,31-Bishomohopane-22R
T30	30,31-Trishomohopane-22S
T31	30,31-Trishomohopane-22R
T32	Tetrakishomohopane-22S
T33	Tetrakishomohopane-22R
T34	Pentakishomohopane-22S
T35	Pentakishomohopane-22R
S4	13b(H),17a(H)-20S-Diacholestane
S5	13b(H),17a(H)-20R-Diacholestane
S8	13b,17a-20S-Methyldiacholestane
S12/S13	14a(H),17a(H)-20S-Cholestane + 13b(H),17a(H)-20S-Ethyldiacholestane
S17/S18	14a(H),17a(H)-20R-Cholestane + 13b(H),17a(H)-20R-Ethyldiacholestane
S18x	Unknown sterane
S19	13a,17b-20S-Ethyldiacholestane
S20	14a,17a-20S-Methylcholestane
S24	14a,17a-20R-Methylcholestane
S25	14a(H),17a(H)-20S-Ethylcholestane
S28	14a(H),17a(H)-20R-Ethylcholestane
S14	14b(H),17b(H)-20R-Cholestane
S15	14b(H),17b(H)-20S-Cholestane
S22	14b,17b-20R-Methylcholestane
S23	14b,17b-20S-Methylcholestane
S26	14b(H),17b(H)-20R-Ethylcholestane
S27	14b(H),17b(H)-20S-Ethylcholestane
RC26/SC27TA	C26,20R- +C27,20S- triaromatic steroid
SC28TA	C28,20S-triaromatic steroid
RC27TA	C27,20R-triaromatic steroid
RC28TA	C28,20R-triaromatic steroid

2.5. Depletion of Steranes

The loss (depletion) of selected dia- and regular steranes in the samples was determined based upon mass losses relative to hopane, which has proven recalcitrant to biodegradation (Prince et al., 1994). The percent depletions of these selected biomarkers in the trap samples were calculated using the following formula:

$$\%\text{Depletion of S} = [((S_0/H_0)-(S_s/H_s))/(S_0/H_0)] \times 100 \quad \text{Eq. (1)}$$

where S_s and H_s are the concentrations of the selected steranes and hopane in the trap sample, respectively, and S_0 and H_0 are the concentrations of the selected steranes and hopane (68.8 μg/g) in the average, fresh Macondo source oil (Stout et al., 2016a). Although hopane can be degraded under some circumstances, if it (H_s) were degraded in a given sample any % depletions calculated are underestimated.

Table 3
Sedimentation rates (flux) of different hydrocarbon measures (see Table 2), mass as dry weight (DW), particulate organic carbon (POC) and biogenic silica (BSi). DW and POC ± standard deviation of replicates. Cups with peak fluxes, representing the four pulses are highlighted in bold with some pulses spanning more than one cup.

Cup #	Mid-date	TPH (μg m^{-2} d^{-1})	TPAH16 (μg m^{-2} d^{-1})	TPAH50 (μg m^{-2} d^{-1})	Hopane (μg m^{-2} d^{-1})	DW (mg m^{-2} d^{-1})	POC (mg m^{-2} d^{-1})	BSi (mg m^{-2} d^{-1})
1	**4-Sep-10**	**1146**	**0.62**	**3.00**	**0.32**	**1618 ± 160**	**109 ± 2**	**397**
2	25-Sep-10	287	0.05	0.54	0.11	663 ± 43	31 ± 0	117
3	16-Oct-10	204	0.05	0.43	0.09	426 ± 18	17 ± 1	44
4	6-Nov-10	240	0.06	0.54	0.12	519 ± 43	22 ± 1	57
5	27-Nov-10	149	0.03	0.36	0.06	283 ± 28	12 ± 0	22
6	**18-Dec-10**	**296**	**0.08**	**1.12**	**0.17**	**671 ± 15**	**22 ± 1**	**47**
7	8-Jan-11	182	0.05	0.43	0.08	467 ± 16	21 ± 0	48
8	29-Jan-11	133	0.04	0.33	0.06	420 ± 24	16 ± 0	39
9	19-Feb-11	104	0.04	0.35	0.05	337 ± 20	13 ± 0	30
10	**12-Mar-11**	**388**	**0.16**	**1.25**	**0.15**	**1282 ± 28**	**38 ± 1**	**119**
11	**2-Apr-11**	**243**	**0.08**	**0.77**	**0.10**	**746 ± 35**	**23 ± 0**	**51**
12	23-Apr-11	136	0.08	0.68	0.09	763 ± 29	29 ± 1	76
13	14-May-11	72	0.04	0.26	0.04	248 ± 9	11 ± 0	22
14	**4-Jun-11**	**75**	**0.05**	**0.30**	**0.04**	**762 ± 54**	**29 ± 0**	**71**
15	**25-Jun-11**	**75**	**0.05**	**0.30**	**0.05**	**440 ± 29**	**19 ± 0**	**51**
16	16-Jul-11	46	0.03	0.16	0.03	291 ± 7	19 ± 3	32
17	6-Aug-11	41	0.03	0.12	0.03	400 ± 30	20 ± 0	59
18	27-Aug-11	56	0.03	0.13	0.04	314 ± 50	14 ± 0	44
19	17-Sep-11	142	0.03	0.04	0.03	384 ± 22	20 ± 0	77

3. Results and discussion

3.1. Flux rates of Macondo Oil, organic carbon, biogenic Silica and mass

Overall, the flux of TPH, TPAH16, TPAH50, and hopane collected in the trap decreased over the entire study period, late August 2010 to September 2011 (6 weeks to 13 months after the end of the spill (Table 3). These overall decreases are consistent with results for a more limited suite of hydrocarbons in these samples previously reported (Yan et al., 2016). Superimposed on this overall decline of different oil-markers, there were four "pulses" of higher sedimentation rates of oil, which can be seen in the temporal trends in the flux of TPH, TPAH50, and hopane (Fig. 2A; Table 3; concentrations of these hydrocarbons in trap samples are presented and discussed in Section 3.2). Each of these show three distinct pulses (Cups 1, 6, 10), as well as the overall decline in the year following the end of the DwH spill. In addition to the three main pulses, a small maximum observed in Cups 14/15 may be considered as a fourth, albeit minor, "pulse" of oil sedimentation. The detailed characteristics of the oil in each of these pulses are discussed in Section 3.2.

POC and mass (DW) flux show the same four pulses (Fig. 2B, Table 3), but not the overall decrease in flux over the annual cycle. Significant correlations between POC and mass flux at depths > 1000 m are well described globally (Armstrong et al., 2002; Francois et al., 2002; Klaas and Archer, 2002; Passow, 2004) and a characteristic of marine carbon flux below 1000 m. Rapidly sinking marine snow collects slowly sinking, small lithogenic and biogenic particles, which in turn may contribute toward ballasting (De La Rocha et al., 2008; Passow and De La Rocha, 2006; Passow et al., 2014). The significant correlations between POC or DW flux and sedimentation rates of oil compounds (e.g. TPAH50 vs. POC; $R = 0.93$, $n = 19$ $p < .001$; or Hopane vs. POC: $R = 0.87$, n = 19, p < .001, reduced major axis correlation) is consistent with the idea that marine snow collects oil compounds from the water column and transports these to depths, as was also observed during laboratory experiments (Passow, 2016; Passow et al., 2019; Passow et al., 2017) and in coagulation models (Dissanayake et al., 2018; Francis and Passow, 2019). Both, mathematical models and lab scale experiments indicate that the amount of oil transported downwards via marine snow is a function of the amounts of marine snow and oil in the water (Francis and Passow, 2019; Passow et al., 2019).

Pulses 1 and 3 (Cups 1 and 10) have the highest mass (> 1 g m^{-2} d^{-1}) and POC fluxes, as well as peak BSi fluxes (Fig. 2B; Table 3). High BSi flux at pulses 1 and 3, and to a lesser extent at Pulse 4, indicates the sedimentation of a diatom bloom, as diatoms have silica frustules, whereas sedimentation pulse 2, which was clearly visible in mass, and to some extent in POC flux, but not in BSi flux must have had a different cause. Microscopic examination (Table 4) of the material characterized by high BSi flux (Cups 1, 10, 15) revealed abundant diatom frustules of especially *Skeletonema* sp. in Cup 1 (Yan et al., 2016), which may have collected only the tail end of a very large diatom sedimentation event (Francis and Passow, 2019). In contrast, Cup 10 contained only few recognizable diatom frustules, but instead an order of magnitude higher concentrations of ellipsoid fecal pellets as well as detrital aggregates, suggesting the diatom bloom was heavily grazed and the BSi sank within feces. The fourth, smaller pulse (Cups 14/15) consisted of a mix of diatoms spanning a range of genera (*Chaetoceros* spp., *Dithylum*, *Rhizosolenia*, centric diatoms), some Radiolaria and Formaninfera as well as fecal and detrital matter, but neither of these particle types were individually significantly above background (e.g. above Cup 19) (Table 4). This fourth sedimentation pulse, prominent in mass, POC and BSi, thus consisted largely of a mix of non-recognizable detrital particles, suggesting intense degradation and grazing activity before the bloom sank or during transit.

Annual vertical flux dynamics in the northern Gulf of Mexico and near the DwH accident site are complex: The site is about 70 km from the Mississippi River delta and clearly influenced by river discharge, which supplies nutrients (nitrogen) that fuel blooms and carries a high load of lithogenic material that is incorporated into sinking POC at a near constant ratio (Giering et al., 2018). On average (2012–2016), POC fluxes at this site peaks in winter/ spring and often an additional summer bloom forms, triggered by river discharge (Giering et al., 2018). Interannual variability in flux at this site is, however, high, and the observed sedimentation pulses between late August 2010 and September 2011 are high, but likely not exceptional, which contrasts the very elevated deposition rates in the months of the active DwH spill

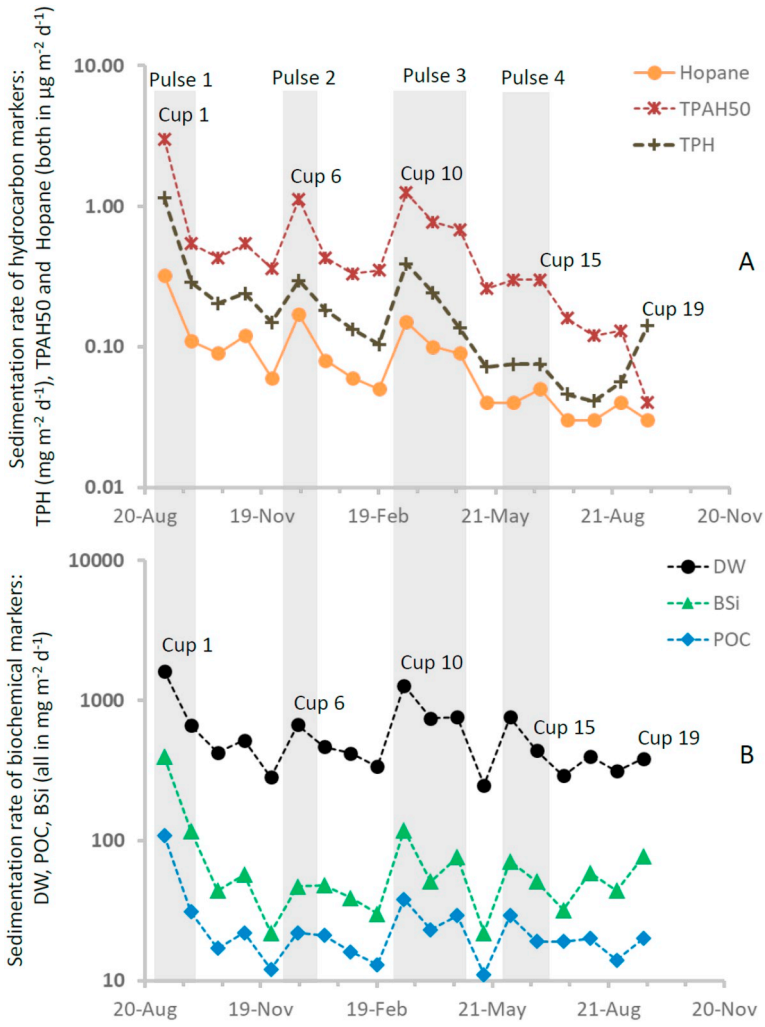

Fig. 2. Flux of (A) hydrocarbon markers and (B) biochemical markers of biogenic particles over time as measured with the sediment trap moored near the DwH spill site from late August 2010 to late September 2011. Hydrocarbon flux as TPH (mg m^{-2} d^{-1}), TPAH50 (µg m^{-2} d^{-1}) and Hopane (µg m^{-2} d^{-1}) (see Table 3) and mass flux (dry weight = DW, mg m^{-2} d^{-1}), particulate organic carbon (POC, mg m^{-2} d^{-1}) and biogenic silica (BSi, (mg m^{-2} d^{-1}). Sedimentation pulses are highlighted with shading. Results from cups representing maximum hopane fluxes during each pulse (Cups 1, 6, 10 and 15) as well as Cup 19 will be presented in detail in the following figures.

(Brooks et al., 2015; Hastings et al., 2016; Larson et al., 2018; Romero et al., 2017). In fact, a reduction in carbon flux for the 6–18 months after the DwH spill ended has been postulated based on a comparison of flux rates in the Viosca Knoll area before and after the DwH spill (2008/9 and 2020/11), respectively; (Prouty et al., 2016).

3.2. Characteristics of oil residues that sank to 1400 m in the months after the spill

3.2.1. Total petroleum hydrocarbons

The GC/FID chromatograms provide chemical fingerprints of the TPH found in the trap samples. Examples of these, specifically representing the four "pulses" in sedimentation described above, are shown in Fig. 3.

The TPH in Cup 1 (Pulse 1) was dominated by a broad unresolved complex mixture (UCM) spanning from around C_{15} to C_{40}, reaching a maximum around C_{34} (Fig. 3A). The UCM is a long-recognized feature of weathered petroleum, e.g. (Gough and Rowland, 1990), indicating the clear presence of weathered crude oil in the Cup 1 sample. Resolved compounds atop the UCM include oil-derived acyclic isoprenoids (pristane and phytane). Shorter-chain n-alkanes are largely absent although longer-chain (n-C_{28}+) n-alkanes are still present. The presence of these long-chain n-alkanes in weathered crude oil is attributed to their lower susceptibility to biodegradation, particularly in marine oil spills (Heath et al., 1997; Peters et al., 2005), which tends to preserve the" waxy" n-alkanes due to steric hindrance effects (Setti et al., 1993). Also present are numerous (mostly) later-eluting resolved compounds, which full scan GC/MS analysis revealed include squalene and multiple (unidentified) unsaturated, highly-branched isoprenoids and cyclic terpenoids (triangles, Fig. 3A). These compounds are biogenic and associated with recent marine biomass (not oil), which was particularly abundant in the Cup 1 due to the sinking (fresh) diatom bloom.

The TPH in Cup 6 (Pulse 2; Dec. 2010) and Cup 10 (Pulse 3; April 2011) also exhibited broad UCMs consistent with weathered crude oil, although their UCMs are somewhat higher boiling than that of Cup 1 (Fig. 3B–C). This is consistent with the Cup 6 and Cup 10 oils being more highly weathered (biodegraded) than the oil in Cup 1, a feature also indicated by the absence of pristane or phytane. In addition to containing a suite of biogenic isoprenoids and terpenoids, the oil in Cups 6 and 10 also contained prominent long-chain n-alkanes ranging

Table 4
Flux of diatom cells and feces in cups 1, 10, 15 and 19.

	Cup # 1; pulse 1	Cup # 10, pulse 3	Cup #15, pulse 4	Cup # 19
Diatom frustules (10^6 cells m^2 d^{-1})	> 8100	6	13	42
Feces (10^3 pellets m^2 d^{-1})	260	2260	620	410

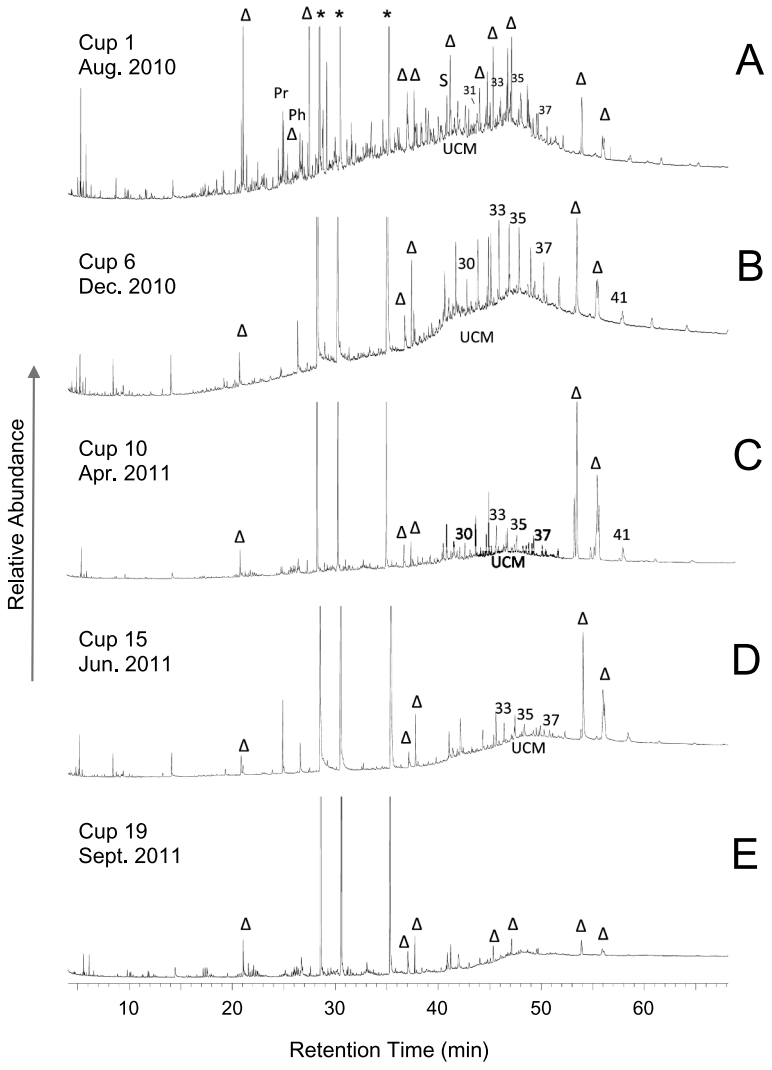

Fig. 3. GC/FID chromatograms for TPH in (A) Cup 1 (Pulse 1; Aug 2010), (B) Cup 6 (Pulse 2; Dec. 2010), (C) Cup 10 (Pulse 3; April 2011), (D) Cup 15 (Pulse 4; June 2011), and (E) Cup 19 (Sept. 2011). * - internal standards; S – squalene; Δ - unidentified unsaturated branched isoprenoids and cyclic terpenoids attributed to biomass (not oil); # - n-alkane carbon number; UCM – unresolved complex mixture.

from about n-C_{28} to n-C_{45}, reaching a maximum around n-C_{33} range (Fig. 3B–C). These long-chain n-alkanes exhibit no odd-over-even predominance typical of modern plant waxes, but instead appear typical of oil. As in the Cup 1 oil, the presence of these long-chain, "waxy" n-alkanes in weathered crude oil is attributed to their preservation during biodegradation (Heath et al., 1997; Setti et al., 1993). In total, the shift in the UCM toward higher masses, the absence of pristane and phytane and the greater prominence of long-chain n-alkanes in the Cup 6 and 10 are all consistent with an increased level of biodegradation of the crude oil arriving at the trap during Pulses 2 and 3 (Cups 6 and 10; Fig. 3B–C), as compared to Pulse 1 (Cup 1; Fig. 3A). The fact that the oil arriving at the trap over time was increasingly biodegraded is consistent with the advancement in weathering of Macondo oil that remained present within the water column – rather than the arrival of some other oil at a single level of weathering such as might be episodically released from natural oil seeps in the region (Stout et al., 2016a).

The TPH recovered from the trap, and represented in Pulses 1, 2 and 3 (Fig. 3A–C), is entirely consistent with weathered oil *droplets*, as evidence by the broad range of hydrocarbons present in proportions consistent with weathered oil. There is no evidence of a preferential abundance of any of the more soluble hydrocarbons in oil, which would indicate sorption of *dissolved*, oil-derived hydrocarbons to sinking particles. The weathered character of the oils found in the trap samples are largely consistent with those exhibited by the oily floc found widespread on the seafloor following the DwH oil spill (Stout and Payne, 2016a; Stout et al., 2016a). The oily floc from the seafloor also similarly weathered and consisted predominantly of a broad UCM, no pristane or phytane, and prominent long-chain n-alkanes, most closely resembling the oil observed in Cup 1 (Fig. 3A). These characteristics (and the PAH and biomarker discussed below) indicate the oil reaching the sediment trap between August 2010 (Fig. 3A) and (at least) April 2011 (Fig. 3C) was weathered Macondo oil comparable to the oily floc deposited on the seafloor throughout the deep-sea. As such, we refer to the oil reaching the sediment trap for months after the DwH spill ended as "lingering" (Macondo) oil.

After April 2011, the trap samples collected contained increasingly lower concentrations of TPH. As such, the GC/FID chromatograms of these later samples contained less-and-less of an UCM and long-chain n-alkanes, and more-and-more biogenic material considered typical of marine biomass. For example, only traces of oil-derived UCM and long-chain n-alkanes are still present in the Cup 15 sample (Pulse 4/June 2011), which is instead dominated by biogenic compounds (see triangles, Fig. 3D). But, although present in low concentrations (Table 5), the trap samples collected after April 2011 (Cups 13 to 18) still contained traces of highly weathered oil. Only the last sample analyzed (Cup 19) contained no recognizable traces of a petroleum-associated

Table 5
Concentrations (μg/g dry) of hydrocarbons in sediment trap samples. Cups representing the four pulses are highlighted in bold with some pulses spanning more than one cup.

Sample	TPH	TPAH16	TPAH50	Hopane	Perylene
Cup 1	**625**	**0.339**	**1.637**	**0.176**	**0.042**
Cup 2	422	0.074	0.791	0.165	0.016
Cup 3	383	0.088	0.803	0.167	0.022
Cup 4	431	0.100	0.970	0.223	0.019
Cup 5	559	0.126	1.358	0.242	0.021
Cup 6	**474**	**0.132**	**1.801**	**0.275**	**0.021**
Cup 7	352	0.093	0.840	0.149	0.017
Cup 8	318	0.092	0.796	0.137	0.015
Cup 9	217 J	0.082	0.719	0.113	0.017
Cup 10	**253**	**0.104**	**0.817**	**0.100**	**0.038**
Cup 11	**308**	**0.097**	**0.982**	**0.122**	**0.027**
Cup 12	172	0.107	0.859	0.108	0.020
Cup 13	182 J	0.092	0.663	0.103	0.019
Cup 14	**137 J**	**0.094**	**0.545**	**0.079**	**0.022**
Cup 15	**155 J**	**0.094**	**0.616**	**0.105**	**0.019**
Cup 16	118 J	0.083	0.418	0.074	0.017
Cup 17	105 J	0.070	0.310	0.067	0.011
Cup 18	123 J	0.066	0.286	0.079	0.014
Cup 19	211	0.048	0.064	0.045	0.017

J - concentration is estimated; below reporting limit.

UCM or long-chain n-alkanes (Fig. 2E). Cup 19's TPH appears entirely attributable to biogenic material and not oil, which is consistent with the low flux of PAHs and hopane at this time (Fig. 2A).

3.2.2. Polycyclic aromatic hydrocarbons (PAHs)

As the flux of total PAHs (TPAH50) declined over time (Fig. 1a), the distribution of individual PAHs in the trap samples also shifted. Fig. 4 shows the individual PAH concentration histograms for the same trap samples that were shown in Fig. 3. Like for TPH, these PAHs exhibit increasing levels of weathering over time. The progression in PAH weathering evident in the Cup 1 through Cup 15 (Fig. 4A–D) is evident in the increasing abundances of higher molecular weight PAHs and PAHs with higher degrees of alkylation. Eventually the high molecular weight benz(a)anthrancenes and chrysenes (BC1-BC3) became the most abundant of the PAHs present (Fig. 4D). This progression is typical of weathering of crude oil due to the combined effects of dissolution and biodegradation, both of which are long recognized to preserve higher molecular weight PAHs with higher degrees of alkylation (Elmendorf et al., 1994). Thus, the PAHs in the oil arriving at the trap over time were increasingly weathered, consistent with a progression in the weathering of "lingering" Macondo oil within the water column.

Cup 1 (Pulse 1) oil contained a prominence of alkylated decalins (D0-D4) that exceeded the concentration of naphthalenes (N0-N4; Fig. 4A). This is notable because the concentration of naphthalenes far exceeds that of decalins in the fresh Macondo oil (Stout et al., 2016b). Naphthalenes are much more soluble and susceptible to biodegradation than decalins, but are comparably volatile to decalins. It is obvious that naphthalenes have been dramatically reduced in the Cup 1 oil compared to decalins (Fig. 4A), which indicates that the oil in this sample has been water-washed and/or biodegraded but not significantly evaporated. Because oil that reached the surface before sinking experienced greater loss of decalins due to evaporation (Stout et al., 2016b), the decalins' relative prominence in the Cup 1 sample's oil indicates that most of the Macondo oil present in Cup 1 could not have come from the sea surface. This indicates that it was predominately-to-exclusively derived from water-washed and/or biodegraded oil from the water column (e.g., deep-sea plume), and not oil that was once at the sea surface. This is consistent with the observation that floating surface oil had dissipated by late August 2010. The same might be concluded for oils in Cups 6 and 10, which also retained traces of decalins and relative absence of naphthalenes, though in declining abundances (Fig. 4B–C). The later arriving oil in Cup 15 was too highly weathered to make this type of distinction.

In contrast to the oil collected in our deep trap, oil collected while the spill was ongoing in shallower traps deployed along the shelf edge, originated from the sea surface, as evidenced by photo-oxidation effects (Stout and German, 2018). Clearly both pathways are possible; oil transported to depth via sinking marine snow may originate either from the surface layer, or from oil dispersed deep in the water column. However, in our study, which was conducted *after* the DwH spill had ended and after any surface slicks had dissipated, it is not surprising to find that the oil reaching our deep trap was oil that had lingered in the water column, and had not reached the sea surface.

The last trap sample studied (Cup 19; Sept. 2011) contained the lowest measured concentration of TPAH50 (0.064 μg/g), most of which was comprised of Priority Pollutant (i.e. non-alkyl substituted) TPAH16 (0.048 μg/g; Table 5; Fig. 4E). Similar to the TPH results, the PAH results also provide no evidence for any oil present in this sample. Instead, the Priority Pollutant PAHs present in this sample at low levels, and the virtual absence of alkylated PAHs, are more reasonably attributed to a "background" deposition of riverine or atmospheric combustion products, which are long known to be enriched in Priority Pollutant PAHs (Blumer and Youngblood, 1975). These substances sink at a low background rate, which may be elevated at the DwH site due to the strong Mississippi influence (Giering et al., 2018).

As was the case with the TPH, the general character of the PAHs in the oil collected by the trap cups closely matches the character of PAHs in the Macondo-derived oily floc found in surface sediments throughout the deep sea. Like in the trap samples (Fig. 4A–D), the average PAH distribution in samples from the seafloor (0–1 cm) also are dominated by C_3– and C_4– alkylated benz(a)anthracenes and chrysenes, with increasingly lower abundances of alkylated fluoranthrenes/pyrenes, phenanthrenes/anthracenes, naphthalenes, and alkylated decalins (Stout and Payne, 2016a). As noted in regard to the TPH, the PAHs in the trap samples also are consistent with the presence of weathered oil *droplets*, and show no evidence of any excess of more soluble PAHs, e.g., naphthalene. The relative prominence of naphthalene in the Cup 1 sample (Fig. 3a) is discussed in the next paragraph. Thus, the sinking oil reaching the trap is consistent with weathered oil droplets, and not dissolved oil-derived compounds that sorbed to sinking particles. We hypothesize that any "lingering" dissolved oil-derived compounds from the DwH spill were likely too diffuse in the months following the active spill, to sorb onto sinking biomass in any measurable concentration.

Unique among the samples studied, Cup 1 contained prominent Priority Pollutant (non-alkylated parent) PAHs, as indicated by the arrows shown in Fig. 4A and the higher TPAH16 concentrations (Table 5). These apparently "extra" non-alkylated PAHs are not reasonably attributable to petrogenic sources and markedly exceed the concentration of Priority Pollutant PAHs present in the Cup 19 "background" sample. Specifically, the TPAH16 sedimentation rate during late August/early September (Cup 1) was 0.62 μg/m^2/d, which is > 10-times higher than the average of all subsequent sampling intervals (0.05 ± 0.03 μg/m^2/day) and 20-times higher than existed one year later (0.03 μg/m^2/day; Table 3). It is well established that Priority Pollutant PAHs, particularly high molecular weight non-alkylated PAHs, are abundant in partially combusted organic matter, including partially combusted oil (Blumer and Youngblood, 1975; Wang et al., 1999). Possible combustion sources related to the *Deepwater Horizon* incident include the original rig fire, increased vessel traffic, and in situ burning (ISB) of floating Macondo oil, the latter of which was used as a countermeasure in response to the spill. We hypothesize that ISB combustion emissions vastly exceeded other sources and therefore, attribute the "extra" Priority Pollutant PAHs in the Cup 1 trap sample (Fig. 4A) to the sedimentation of combustion particles derived from ISB. Specifically, between April 28 and July 19, 2010 approximately 220,500 to 310,400 barrels (bbls) of floating Macondo crude oil reportedly were consumed in 411 separate ISB events (Mabile, 2010; Perring et al., 2011). At least some fraction of

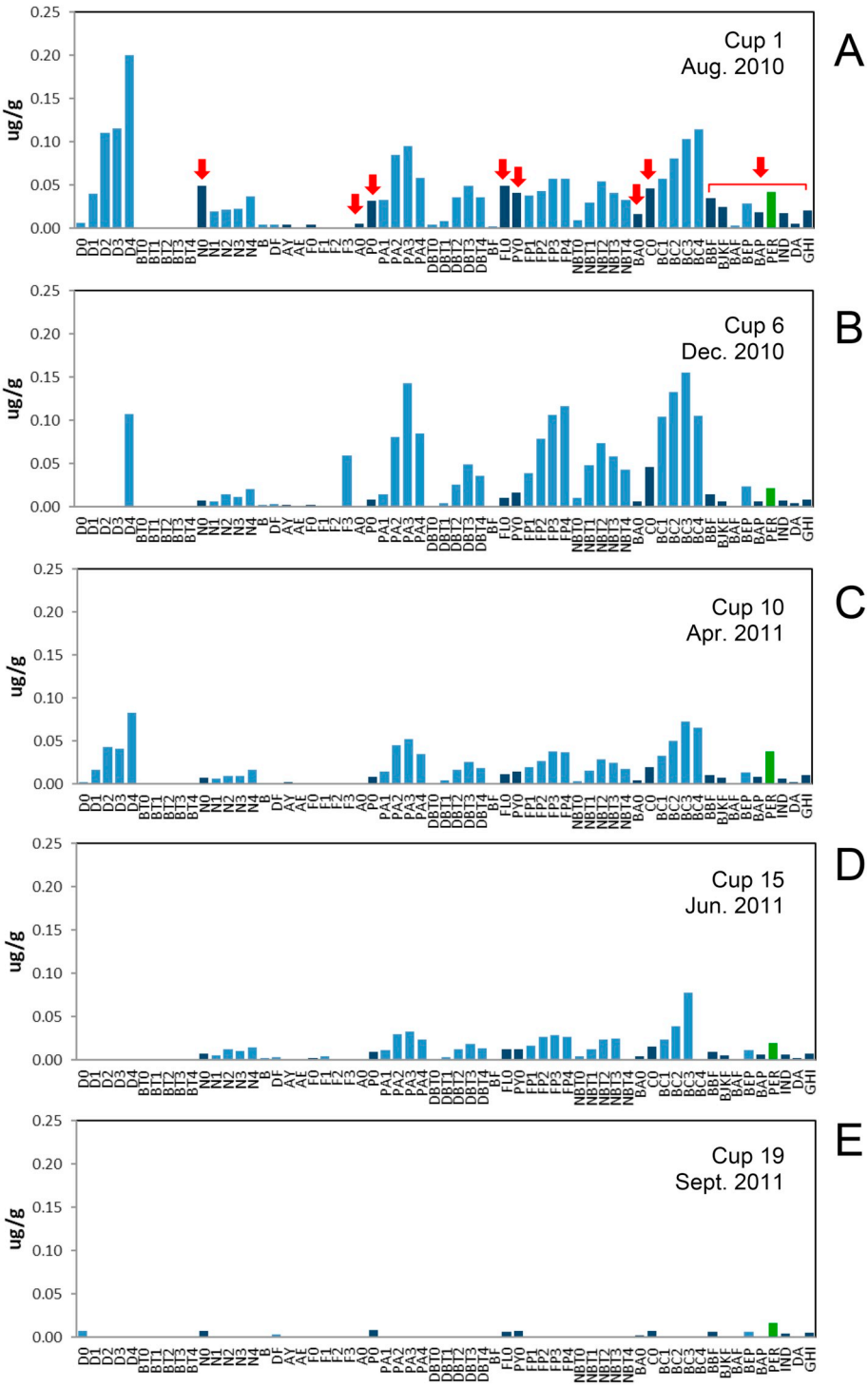

Fig. 4. Histograms of PAH concentrations in (A) Cup 1 (Pulse 1; Aug 2010), (B) Cup 6 (Pulse 2; Dec. 2010), (C) Cup 10 (Pulse 3; Mar. 2011), (D) Cup 15 (Pulse 4; June 2011), and (E) Cup 19 (Sept. 2011). All concentrations in (μg / g dry wt). For compound abbreviations see Table 2. Dark blue bars indicate Priority Pollutant PAH used in calculating TPAH16. Green bar is perylene attributed largely to biomass, not oil. Arrows indicate excess Priority Pollutant PAHs in Cup 1 sample attributed to combustion-derived particles from in-situ burning during DwH spill response. (For interpretation of the references to colour in this figure legend, the reader is referred to the web version of this article.)

the uncombusted emissions from these fires returned to the sea surface and settled through the water column. Indeed, macroscopic pieces of sunken burn residues collected from the seafloor following the DwH events were also enriched in Priority Pollutant PAHs (Stout and Payne, 2016b). The "extra" Priority Pollutants present in the late August-early September trap material (Cup 1; Fig. 4A; Table 5) thereby likely reflects microscopic combustion particles from the ISB events, a conclusion supported by measurements of black carbon in the Cup 1 sample (Yan et al., 2016). The fact that the last ISB events occurred in mid-July 2010, and that "extra" Priority Pollutant PAHs were not observed after late August-early September (Cup 1), indicates that combustion particles from the ISB events apparently "lingered" in the atmosphere or water column for 5 or 6 weeks. Likely their residence time in the water is determined by the frequency of large sedimentation events that carry these substances to depths. Our results suggest that the large diatom event responsible for Pulse 1 was sufficient to "clean" the water column of these lingering combustion particles.

Finally, it is notable that the absolute concentration of perylene in the trap samples was generally constant throughout the sampling period except for those samples collected in Cups 1 and 10, which contained about twice as much perylene as the other samples (Table 5, Fig. 4). Perylene is considered a biogenic PAH, derived from multiple sources of biomass, including diatoms (e.g., Venkatesan, 1988). BSi fluxes were highest in Cups 1 and 10 (Pulse 1 and 3) indicating the

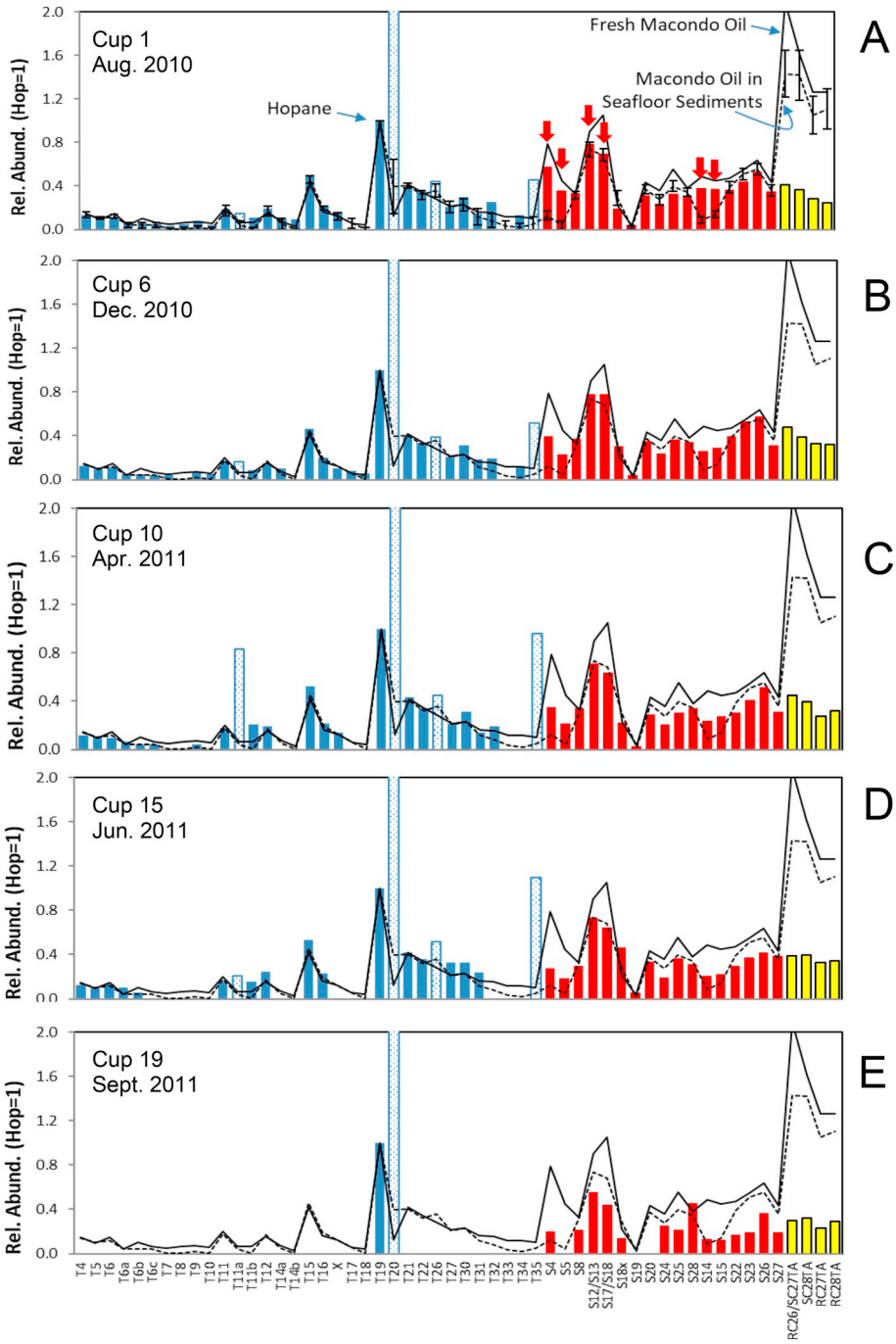

Fig. 5. Histograms showing hopane-normalized distributions of triterpanes (blue), steranes and diasteranes (red), and triaromatic steroids (TAS; yellow) in (A) Cup 1 (Pulse 1; Aug 2010), (B) Cup 6 (Pulse 2; Dec. 2010), (C) Cup 10 (Pulse 3; Mar. 2011), (D) Cup 15 (Pulse 4; June 2011) and (E) Cup 19 (Sept. 2011). For compound abbreviations see Table 2. Light blue stipple indicates naturally-occurring (terpanoid) interferences with target analytes. Distributions for fresh Macondo oil and average seafloor floc containing Macondo oil in surface (0–1 cm) sediments 4.8 to 8.0 km from the wellhead (Stout and Payne, 2016a) are shown for comparison. Arrows indicate biodegradation susceptible C27 βα-diasteranes (S4 and S5) and C27ββ-steranes (S14 & S15); loss of C27 αα-steranes (S12 and S17) is suspected but confounded by co-elutions; see text. Solid black lines depict average for fresh Macondo oil (Stout et al., 2016b); Dashed black lines depict average for surface sediments 4.8 to 8.0 km from Macondo well (Stout and Payne, 2016a). Error bars in (A) = 1σ. (For interpretation of the references to colour in this figure legend, the reader is referred to the web version of this article.)

sedimentation of diatom biomass. Sinking diatom blooms are frequently responsible for maximal sedimentation rates, and it is therefore perhaps not surprising that Cups 1 and 10 (Pulses 1 and 3) each, which had the highest concentrations of perylene and BSi, also contained the highest total masses of particulate material measured as dry weight (Fig. 2B, Table 3).

3.2.3. Petroleum biomarkers

As noted above, hopane concentrations in the trap samples decreased over the sampling period with minor increases generally coincident with “pulses” in TPH and PAH (Fig. 2A; Table 5). Hopane, of course, is only one of the targeted biomarkers present in crude oil (Table 2) and in this case hopane was the most abundant biomarker detected. Its dominance can be seen in Fig. 5, which shows hopane-normalized histograms of all targeted biomarkers in the same five trap samples shown in Figs. 3 and 4. For comparison, also shown in Fig. 5 are the average biomarker distributions for fresh Macondo oil (Stout et al., 2016b) and for Macondo oily floc collected from the seafloor surface (0–1 cm) of 20 cores 4.8 to 8.0 km from the Macondo well (Stout and Payne, 2016a).

There is an overall similarity between the biomarkers in the trap samples and those of fresh Macondo oil and/or oily floc collected from the seafloor. However, there are some notable differences for each of the three classes of biomarkers studied, viz., triterpanes (blue), diasteranes and steranes (red), and triaromatic steroids (TAS; yellow; Fig. 5). The observed differences of biomarkers are attributable to (1) interferences with biomarkers derived from recent marine biomass in the trap samples and (2) the effects of weathering, viz., biodegradation and dissolution, as explained in the following paragraphs.

Various terpenoids were clearly evident in the GC/FID

chromatograms of the trap samples (Fig. 3). Recent sediments contain terpenoids derived from modern algal and/or microbial biomass, including numerous hopenes and 17β(H),21β(H)-hopanes (Hood et al., 2002; Simoneit, 1986). These modern terpenoids can interfere and co-elute with targeted (oil-derived) biomarkers within *m/z* 191 mass chromatograms (not shown; Dembicki, 2010). Under the GC/MS conditions used for this study modern terpenoids co-elute with at least four targeted biomarkers (T11a, T20, T26, and T35; Table 2), which are indicated by the light-blue stippled bars in Fig. 5. The largest of these occurs at T20 (moretane; Fig. 5) and is likely due to the co-elution of 17β(H),21β(H)-30-norhopane, a naturally-occurring triterpane, which can be prominent in recent marine sediments (Kennicutt and Comet, 1992). Thus, the prominence of these modern terpenoids (mostly biohopanoids) in the trap samples is attributed to modern biomass - and not the presence of a "different" type of crude oil.

Minor differences in sterane distributions are also likely affected by the presence of modern marine biomass in the trap material. However, significant differences between the trap samples and fresh Macondo oil and seafloor floc containing Macondo oil appear in the relative abundances of C_{27} βα-diasteranes (S4 and S5) and C_{27} ββ-steranes (S14 and S15; Table 2; Fig. 5). The abundances of these compounds in the trap samples appear intermediate between the fresh Macondo oil and oily floc from the seafloor. In addition, the relative abundances of these diasteranes and steranes tend to decrease in the trap samples over time. This temporal trend can be seen in the examples of trap oils shown in Fig. 5A through 5D, but is more easily seen in Fig. 6, which shows the calculated percent depletions of C_{27} βα-diasteranes (S4 and S5) and C_{27} ββ-steranes (S14 and S15) for all 19 of the trap samples studied. The progressive loss of these compounds is clearly evident in Cups 1 through 8 (late August 2010 to late January 2011) and appears to continue, albeit with some scatter, thereafter (Fig. 6). As is evident in Fig. 4 (see black dashed lines), the C_{27} βα-diasteranes and C_{27} ββ-steranes were significantly depleted within the widespread oily floc found in surface sediments (Stout and Payne, 2016a; Stout et al., 2016a). A comparable loss of βα-diasteranes and ββ-steranes was also reported by White and coauthors (2012) for the oily floc found coating deep-sea corals from northeast Biloxi Dome in later 2010. The preferential loss of C_{27} βα-diasteranes and/or C_{27} ββ-steranes has been previously observed in highly biodegraded oils from the environment (Prince et al., 1994; Prince et al., 2002; Wang et al., 2001) and in vitro (Dıez et al., 2005). Thus, these compounds' progressive depletion in sinking oil is evidence that biodegradation of the "lingering" Macondo oil occurred within the water column after the spill ended. This progressive loss of C_{27} βα diasteranes and ββ-steranes is consistent with the progressively weathered character of the TPH and PAH present in the trap samples, and demonstrates the oil arriving at the trap was progressively weathered within the water column in the months following the end of the DwH spill.

Finally, the most obvious difference between the biomarkers in the oil from trap material and fresh Macondo oil or oily floc found in seafloor sediment samples throughout the area (Fig. 1) is the significant depletion of all four TAS congeners measured in the trap material (see yellow bars; Fig. 5). The cause for this difference is elucidating given the otherwise high similarity between the oil from trap samples and from the seafloor. Given their condensed aromatic structures, TAS are considered susceptible to photo-oxidation and were observed to be variably depleted in floating and stranded Macondo oils (Aeppli et al., 2014; Stout et al., 2016b). Therefore, photo-oxidation was first suspected to explain the depletion of TAS. However, photo-oxidation also affects other *uv*-sensitive compounds (Garrett et al., 1998). Indeed, floating oils collected during the DwH spill exhibited preferential losses of specific higher molecular weight PAH isomers considered susceptible to photo-oxidation (e.g., benz(a)anthracene and selected methyl-chrysene, methyl-fluoranthene/pyrene, and benzofluorene isomers; Stout et al., 2016b). As noted above, sediment trap oil collected near the shelf edge during the active DwH spill exhibited evidence of photo-oxidation of higher molecular weight PAH isomer (Stout and German, 2018). However, upon inspection of PAH isomer patterns evidence for photo-oxidation was lacking. For example, the sediment trap oils studied herein do not exhibit a loss of benz(a)anthracene relative to chrysene (Fig. 3), which was evident in both floating oils (Stout et al., 2016b) and sediment trap oils obtained during the active spill (Stout and German, 2018). In addition, Fig. 7 shows the distributions of methyl-chrysene (MC) isomers for selected samples. Whereas those isomers most susceptible to photo-oxidation (2-, 6-, and 1-MC) were reduced relative to fresh Macondo oil in previously-studied floating oils (Stout et al., 2016b; Fig. 7B), the sediment trap oils from the four pulses of oil sedimentation are not (Fig. 7C–F). Instead the sediment trap oils more closely resemble oily floc from the seafloor (Fig. 7G). This argues that photo-oxidation could not reasonably explain the depleted TAS in our trap samples (Fig. 5). Furthermore, photo-oxidation would mandate that the oil reaching our trap had once been at the sea surface, which does not seem likely given the general lack of evaporation of the decalins (Fig. 4A; described above). Evaporation of the TAS can also be ruled out given the lack of evaporation among many more volatile constituents in the trap samples.

This leaves biodegradation or dissolution as possible causes for the depletion of TAS within the trap samples. Both processes could have affected the Macondo oil arriving at the trap. Because the sedimentation events presented here occurred many weeks after the leak was sealed, the oil collected in the trap, represent "lingering" oil droplets that remained within the water column long after its release. This "lingering" oil may have experienced a great degree of dissolution and biodegradation due to its residence in the water column, before being scavenged by sinking marine snow. Both dissolution and biodegradation of TAS would be enhanced, especially if the "lingering" oil

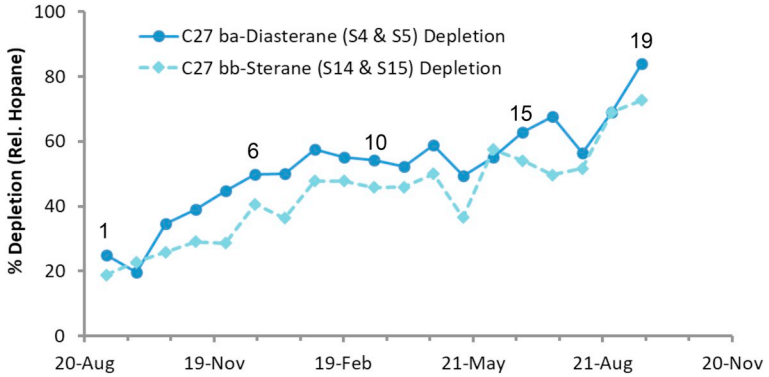

Fig. 6. Plot showing percent depletions (relative to hopane; Eq. (1)) of C27 βα-diasteranes and C27 ββ-steranes in sediment trap samples over time. Increased depletion over time shows progressive biodegradation of these biomarkers occurred in the water column. Selected cup numbers are indicated.

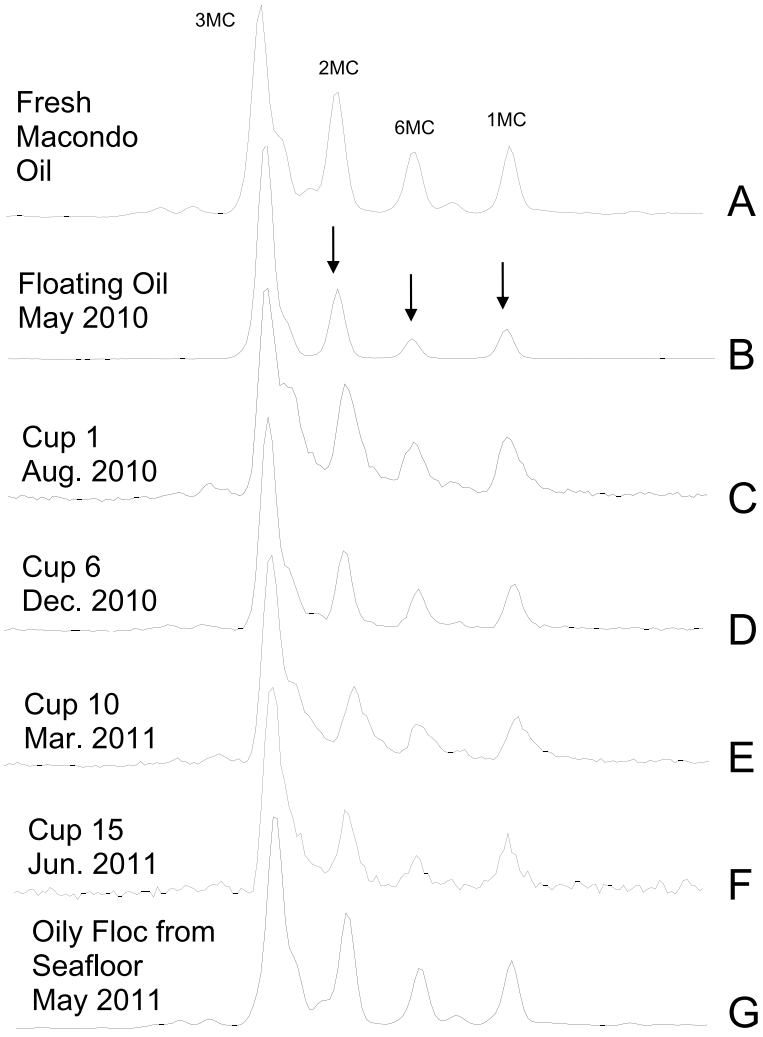

Fig. 7. Partial extracted ion profiles showing methyl-chrysene isomers (*m/z* 242) in (A) fresh Macondo oil, (B) floating Macondo oil affected by photo-oxidation, (C) Cup 1 (Pulse 1; Aug 2010), (D) Cup 6 (Pulse 2; Dec. 2010), (E) Cup 10 (Pulse 3; March 2011), (F) Cup 15 (June 2011), and (G) oily floc from the seafloor. (A) and (B) from Stout et al. (2016b); (G) from Stout and Payne, 2016a; (SB9-65-B0528-S-LBNL3-HC-0929 collected ~1 km NE of the sediment trap; Fig. 1). All panels are plotted normalized to the peak height of 3-methyl-chrysene (3MC). The arrows in (B) show reduced abundances of the isomers more susceptible to photo-oxidation, including 2-methyl, 6-methyl, and 1-methyl-chrysene (2MC, 6MC, and 1MC).

consisted of small droplet sizes, because the larger surface area-to-volume ratios, allows for greater dissolution and/or biodegradation to occur. We thus hypothesize that the greater depletion of TAS within the trap samples versus TAS in seafloor oily floc (Fig. 5) lies in the longer residence time of oil transported to depth many weeks to months after the spill compared to the oily floc sampled from the seafloor, which consisted of a large fraction of oil transported more quickly to the seafloor while the spill was ongoing. Very high deposition and accumulation rates at the seafloor would reduce, on average, dissolution or biodegradation of the deposited oily floc, as bioturbation and resuspension would be reduced. The large mass of oily floc that accumulated during the three months of the active spill would dilute the signal of a smaller mass deposited after the spill ended, the latter of which is represented by our trap samples.

4. Summary and conclusion

In summary, the detailed chemical character of the TPH, PAHs, and petroleum biomarkers collected in a sediment trap at 1400 m depth near the DwH site approximately 6 weeks to 13 months after the spill ended in July 2010, is consistent with droplets of weathered Macondo crude oil. The lack of evaporation and photo-oxidation indicated the oil arriving at the trap between late August 2010 and June 2011 was derived overwhelmingly (perhaps exclusively) from oil droplets that lingered (and continued to weather) in the water column. This "lingering" Macondo oil was collected by sinking marine snow during several large sedimentation events that transported the biomass and the oil to the seafloor, and progressively "cleaned" the water column within ~13 months after the end of the DwH spill. Three of these sedimentation events (Pulses 1, 3, 4) were the consequence of diatom blooms, the second sedimentation pulse had another origin(s); possibly a sinking *Trichodesmium* bloom or a grazed picoplankton bloom. Whereas the first sedimentation pulse (late August 2010) was caused by the direct sinking of diatom aggregates, which, previous experiments revealed will efficiently incorporate dispersed oil droplets (Passow, 2016; Passow et al., 2017, 2019), the third sedimentation pulse (April 2011) was dominated by sinking fecal and detrital material originating from the grazing of a diatom bloom. Zooplankton, depending on size and type, graze on cells directly or on phytoplankton aggregates; many are suspension feeders, and some indiscriminate feeders that would ingest oil droplets directly. Thus zooplankton feces and feeding structures contain oil if grazing occurs in oil contaminated water (Almeda et al., 2015; Fernández-Carrera et al., 2016; Mitra et al., 2012). Whatever the exact mechanism of oil incorporation into sinking feces and detrital aggregates, it was clearly an effective method to sink "lingering" oil and strip the water column progressively of this lingering oil. The removal rate of such oil lingering in the water is thus in part a function of the frequency and magnitude of sedimentation events.

Resuspension of oil deposited upslope could have contributed to the oil in the water (Diercks et al., 2018), but there were no biological or isotopical indications that resuspension was of major importance during the time series discussed here (Yan et al., 2016; Giering et al., 2018; Chanton et al., 2018).

Although varying in the exact mechanism(s) involved, all four

sedimentation events were driven by high primary productivity that surpassed recycling activity in the surface ocean, thus leading to particle export pulses out of the surface layer of the ocean. Scavenging and transport of increasingly weathered Macondo oil droplets that lingered in the water by sinking aggregates or feces was inadvertent, and not caused directly by the presence of the weathered oil. In contrast, the massive sedimentation of oily floc during the active spill was caused by a series of different types of marine snow events, including some that were caused directly by the presence of oil, such as the formation of biofilm-like microbial mucous-rich marine snow (Passow and Ziervogel, 2016). The presence of large amounts of Macondo oil during the active spill led to a large bacterial response, which resulted in the formation of bacterial agglomerations (Baelum et al., 2012; Doyle et al., 2018; Hazen et al., 2010), including many that were large enough to sink at significant speeds during the active DwH spill (Passow, 2016; Passow et al., 2012; Ziervogel et al., 2012).

All four sedimentation pulses in the year following the end of the DwH spill, although they differed, also transported oil to depths at overall decreasing flux rates. The first sedimentation event after the DwH ended (September 2010) also transported Priority Pollutant PAH-rich (TPAH16) combustion particles, likely "lingering" within the water column following in-situ burning conducted during the spill's response, to the seafloor. Because the last in situ burning occurred July 19 (~5–6 weeks prior to late August/early September), the TPAH16 sedimentation rate(s) prior to late August, and certainly during the active ISB events, were likely much higher.

A comparison of oil composition in trap samples with oily floc deposited on the seafloor emphasizes the high degree of similarity, largely due to the very high deposition rates of marine snow during the active spill. The only significant difference among the oil collected in trap and oily floc from the seafloor was the reduced abundance of TAS in the former, which may be explained by greater dilution and biodegradation of oil droplets lingering in the water column compared to those deposited more rapidly on the seafloor during the active spill's massive marine snow events.

Based upon the combined evidence of the overall declining oil sedimentation rates following the end of the spill, and the character and progression in weathering of the oil that reached the trap over time, it is evident that "lingering" Macondo oil was still present in the water column, and being transported to the seafloor over the time period spanning from late August 2010 (Cup 1) to late August 2011 (Cup 18). This means that "lingering" Macondo oil droplets were still being transported to the seafloor for up to 13 months after the DwH spill had ended. These results are consistent with the observation that flux rates of petrogenic hydrocarbons were even less prevalent in 2012 (Giering et al., 2018). The recovery period at the DwH spill site was longer, near 3 years, when $\Delta^{14}C$ was used as an indicator (Chanton et al., 2018). Longer residency time of petrocarbon products based on isotopic signature reflected higher methodological sensitivity, and the fact that new biomass formed from petrocarbon, would carry the fossil $\Delta^{14}C$ signature. The overall decline in oil sedimentation rates over time may be attributed to increasingly less Macondo oil remaining in the water column above the trap due to progressive "sweeping" of the water column with each sedimentation event, along with continued weathering and dilution.

This and other sediment trap studies were able to show – for the first time during DwH – that sedimentation of oil via marine snow can be a significant transport and distribution pathway. Experimental (Passow et al., 2019) and sediment trap results now allow us to formulate models, which have predictive power (Dissanayake et al., 2018; Francis and Passow, 2019) and may provide the first step to include this process in response models and planning. Moreover, deployment of sediment traps in the future near sites of deep oil spills will contribute toward assessment of the fate of oil and its distribution in marine ecosystems.

Acknowledgements

This research was supported by two "Rapids" from the National Science Foundation (OCE 1045330 & OCE 1059103) to U.P., by a grant from The Gulf of Mexico Research Initiative (GoMRI) to support the consortia ECOGIG (Ecosystem Impacts of Oil and Gas Inputs to the Gulf), as well as by NOAA as part of the NRDA process to S.S. U.P. was additionally funded by the Multi Partner Oil Research, Canada. The original biogenic trap data can be found at the Gulf of Mexico Research Initiative Information and Data Cooperative (GRIIDC) under doi: R4-x268-184-0001; the chemical concentration data are available in the Supporting Information to this study. This is ECOGIG contribution # XXX.

The scientific results and conclusion of this publication, as well as any views or opinions expressed herein, are those of the authors only. The authors declare no competing financial interest in the publication of this study.

Appendix A. Supplementary data

Supplementary data to this article can be found online at https://doi.org/10.1016/j.marchem.2019.103733.

References

Aeppli, C., et al., 2014. Recalcitrance and degradation of petroleum biomarkers upon abiotic and biotic natural weathering of Deepwater horizon oil. Environ. Sci. Technol. 48, 6726–6734.
Alldredge, A.L., Silver, M.W., 1988. Characteristics, dynamics, and significance of marine snow. Prog. Oceanogr. 20, 41–82.
Almeda, R., Connelly, L., Buskey, E., 2015. How much crude oil can zooplankton ingest? Estimating the quantity of dispersed crude oil defecated by planktonic copepods. Environ. Pollut. 208.
Armstrong, R.A., Lee, C., Hedges, J.I., Honjo, S., Stuart, W.G., 2002. A new mechanistic model for organic carbon fluxes in the ocean based on the quantitative association of POC with ballast minerals. Deep-Sea Res. II 49, 219–236.
Baelum, J., et al., 2012. Deep-sea bacteria enriched by oil and dispersant from the Deepwater Horizon spill. Environ. Microbiol. 14 (9), 2405–2416.
Blumer, M., Youngblood, W.W., 1975. Polycyclic aromatic hydrocarbons in soils and recent sediments. Science 188, 53–55.
Boehm, P.D., Murray, K.J., Cook, L.L., 2016. Distribution and attenuation of polycyclic aromatic hydrocarbons in Gulf of Mexico seawater from the Deepwater Horizon oil accident. Environ. Sci. Technol. 50 (2), 584–592.
Brooks, G.R., et al., 2015. Sedimentation pulse in the NE Gulf of Mexico following the 2010 DWH blowout. PLoS One 10 (7), e0132341.
Camilli, R., et al., 2010. Tracking hydrocarbon plume transport and biodegradation at Deepwater Horizon. Science 330, 201): 201–204.
Chanton, J., et al., 2015. Using natural abundance radiocarbon to trace the flux of Petrocarbon to the seafloor following the Deepwater horizon oil spill. Environ. Sci. Technol. 49 (2), 847–854.
Chanton, J.P., et al., 2018. Isotopic composition of sinking particles: oil effects, recovery and baselines in the Gulf of Mexico, 2010–2015. Elem. Sci. Anth. 6 (1), 43.
Daly, K.L., Passow, U., Chanton, J., Hollander, D., 2016. Assessing the impacts of oil-associated marine snow formation and sedimentation during and after the Deepwater horizon oil spill. Anthropocene 13, 18–33.
De La Rocha, C.L., Nowald, N., Passow, U., 2008. Interactions between diatom aggregates, minerals, particulate organic carbon, and dissolved organic matter: Further implications for the ballast hypothesis. Glob. Biogeochem. Cycles 22, GB4005.
DeMaster, D., 1981. The supply and accumulation of silica in the marine environment. Geochim. Cosmochim. Acta 45, 1715–1732.
Dembicki, H., 2010. Recognizing and compensating for interference from sediment's background organic matter and biodegradation during interpretation of biomarker data from seafloor hydrocarbon seeps, An example from the Marco Polo area seeps, Gulf of Mexico, USA. Mar. Pet. Geol. 27, 1936–1951.
Diercks, A.-R., Dike, C., Asper, V., DiMarco, S.F., Chanton, J., Passow, U., 2018. Scales of seafloor sediment resuspension in the northern Gulf of Mexico. Elem. Sci. Anthropocene 6, 32. https://doi.org/10.1525/elementa.285.
Díez, S., et al., 2005. The Prestige oil spill. I. Biodegradation of a heavy fuel oil under simulated conditions. Environ. Toxicol. Chem. 24, 2203–2217.
Dissanayake, A.L., Burd, A.B., Daly, K.L., Francis, S., Passow, U., 2018. Numerical Modeling of the interactions of oil, marine snow, and riverine sediments in the ocean. J. Geophys. Res. Oceans 123 (8), 5388–5405.
Douglas, G.S., Emsbo-Mattingly, S.D., Stout, S.A., Uhler, A.D., McCarthy, K.J., 2015. In: Murphy, B.L., Morrison, R.D. (Eds.), Introduction to Environmental Forensics, 3rd Ed. Academic Press, Boston, pp. 201–309.
Doyle, S.M., et al., 2018. Rapid formation of microbe-oil aggregates and changes in community composition in coastal surface water following exposure to oil and the dispersant Corexit. Front. Microbiol. 9 (689).
Elmendorf, D.L., Haith, C.E., Douglas, G.S., Prince, R.C., 1994. Relative rates of biodegradation of substituted polycyclic aromatic hydrocarbons. In: Hinchee, A.E.S.R.E.L., Ong, L., Ann Arbor, S.K. (Eds.), Bioremediation of Chlorinated and PAH Compounds.

Lewis Publishers, Michigan, pp. 188–202.
Fernández-Carrera, A., Rogers, K., Weber, S., Chanton, J., Montoya, J., 2016. Deep Water Horizon oil and methane carbon entered the food web in the Gulf of Mexico. Limnol. Oceanogr. 61 (S1).
Fisher, C.R., et al., 2014. Footprint of Deepwater Horizon blowout impact to deep-water coral communities. In: Proceedings of the National Academy of Sciences.
Fisher, C.R., Montagna, P.A., Sutton, T., 2016. How did the Deepwater horizon oil spill impact deep-sea ecosystems? Oceanography 29 (3), 182.
Francis, S., Passow, U., 2019. Transport of dispersed oil to the seafloor by sinking phytoplankton aggregates: a modeling study. Deep Sea Research, submitted.
Francois, R., Honjo, S., Krishfield, R., Manganini, S., 2002. Factors controlling the flux of organic carbon to the bathypelagic zone of the ocean. Glob. Biogeochem. Cycles 16, (4): 1087.
Garrett, R.M., Pickering, I.J., Haith, C.E., Prince, R.C., 1998. Photooxidation of crude oils. Environ. Sci. Technol. 32 (23), 3719–3723.
Giering, S., et al., 2018. An ecosystem baseline of particle flux in the Northern Gulf of Mexico. Elem. Sci. Anthropocene 6 (1).
Gong, Y., et al., 2014. A review of oil, dispersed oil and sediment interactions in the aquatic environment: influence on the fate, transport and remediation of oil spills. Mar. Pollut. Bull. 79 (1–2), 16–33.
Gough, M.A., Rowland, S.J., 1990. Characterization of unresolved complex mixtures of hydrocarbons in petroleum. Nature 344, 648–650.
Hastings, D.W., et al., 2014. Changes in sediment redox conditions following the BP DWH blowout event. In: Deep Sea Research Part II: Topical Studies in Oceanography.
Hastings, D.W., et al., 2016. Changes in sediment redox conditions following the BP DWH blowout event. Deep-Sea Res. II Top. Stud. Oceanogr. 129, 167–178.
Hazen, T.C., et al., 2010. Deep-Sea oil plume enriches indigenous oil-degrading Bacteria. Science 330 (6001), 204–208.
Heath, D.J., Lewis, C.A., Rowland, S.J., 1997. The use of high temperature gas chromatography to study the biodegradation of high molecular weight hydrocarbons. Org. Geochem. 26, 769–785.
Hood, K.C., Gross, O.P., Wenger, L.M., Harrison, S.C., 2002. Hydrocarbon systems analysis of the northern Gulf of Mexico: delineation of hydrocarbon migration pathways using seeps and seismic imaging. AAPG Stud. Geol. 48, 25–40.
Jackson, G.A., 2005. Coagulation theory and models of oceanic plankton aggregation. In: Droppo, I., Leppard, G., Liss, S., Milligan, T. (Eds.), Flocculation in Natural and Engineered Environmental Systems. CRC Press, Bocca Raton, Florida, pp. 284–305.
Kennicutt, M.C., Comet, P.A., 1992. Resolution of sediment hydrocarbons sources: Multiparameter approach. In: Organic Matter: Productivity, Accumulation, and Preservation in Recent and Ancient Sediments. Columbia Univ. Press, New York.
Klaas, C., Archer, D.E., 2002. Association of sinking organic matter with various types of mineral ballast in the deep sea: implications for the rain ratio. Global Biochem. Cycles 16 (4), 1116.
Kumar, M.D., Sarma, V.V.S.S., Ramaiah, N., Gauns, M., de Sousa, S.N., 1998. Biogeochemical significance of transparent exopolymer particles in the Indian Ocean. Geophys. Res. Lett. 25, 81–84.
Larson, R.A., et al., 2018. High-resolution investigation of event driven sedimentation: Northeastern Gulf of Mexico. Anthropocene 24, 40–50.
Lee, K., 2002. Oil-particle interactions in aquatic environments: influence on the transport, fate, effect and remediation of oil spills. Spill Sci. Amp; Technol. Bull. 8 (1), 3–8.
Long, M., et al., 2015. Interactions between microplastics and phytoplankton aggregates: impact on their respective fates. Mar. Chem. 175, 39–46.
Mabile, N.a.A.,A, 2010. Controlled Burns - After-action Report.
Mitra, S., et al., 2012. Macondo-1 well oil-derived polycyclic aromatic hydrocarbons in mesozooplankton from the northern Gulf of Mexico. Geophys. Res. Lett. 39 (L01605).
Montagna, P., et al., 2013. Deep-Sea benthic footprint of the Deepwater horizon blowout. PLoS One 8 (8), e70540.
Mortlock, R.A., Froelich, P.N., 1989. A simple method for the rapid determination of biogenic opal in pelagic marine sediments. Deep-Sea Res. 36, 1415–1426.
Murawski, S.A., Hogarth, W.T., Peebles, E.B., Barbeiri, L., 2014. Prevalence of external skin lesions and polycyclic aromatic hydrocarbon concentrations in Gulf of Mexico fishes, post-Deepwater horizon. Trans. Am. Fish. Soc. 143 (4), 1084–1097.
Passow, U., 2004. Switching perspectives: do mineral fluxes determine particulate organic carbon fluxes or vice versa. Geochem. Geophys. Geosyst. 5 (4), 1–5.
Passow, U., 2016. Formation of rapidly-sinking, oil-associated marine snow. Deep-Sea Res. II Top. Stud. Oceanogr. 129, 232–240.
Passow, U., De La Rocha, C.L., 2006. Accumulation of mineral ballast on organic aggregates. Glob. Biogeochem. Cycles 20 (GB1013), 7.
Passow, U., Ziervogel, K., 2016. Marine snow sedimented oil released during the Deepwater Horizon spill. Oceanography 29 (3), 118–125.
Passow, U., et al., 2001. Origin of transparent exopolymer particles (TEP) and their role in the sedimentation of particulate matter. Cont. Shelf Res. 21, 327–346.
Passow, U., Ziervogel, K., Asper, V., Diercks, A., 2012. Marine snow formation in the aftermath of the Deepwater Horizon oil spill in the Gulf of Mexico. Environ. Res. Lett. 7 (35031), 11.
Passow, U., Rocha, C.L.D.L., Fairfield, C., Schmidt, K., 2014. Aggregation as a function of pCO2 and mineral particles. Limnol. Oceanogr. 59 (2), 532–547.
Passow, U., Sweet, J., Quigg, A., 2017. How the dispersant Corexit impacts the formation of sinking marine oil snow. Mar. Pollut. Bull. 125 (1–2), 139–145.
Passow, U., et al., 2019. Incorporation of oil into diatom aggregates. Mar. Ecol. Prog. Ser. 612, 65–86.
Payne, J.R., Driskell, W.B., 2018. Macondo oil in northern Gulf of Mexico waters – part 1: assessments and forensic methods for Deepwater Horizon offshore water samples. Mar. Pollut. Bull. 129 (1), 399–411.
Perring, A.E., et al., 2011. Characteristics of black carbon aerosol from a surface oil burn during the Deepwater Horizon oil spill. Geophys. Res. Lett. 38 (L17809), 5pp.
Peters, K.E., Walters, C.C., Moldowan, J.M., 2005. Biomarkers and isotopes petroleum systems and Earth history., II. In: The Biomarker Guide. Cambridge Univ. Press, Cambridge.
Prince, R.C., et al., 1994. 17a(H),21b(H)-hopane as a conserved internal marker for estimating the biodegradation of crude oil. Environ. Sci. Technol. 28 (1), 142–145.
Prince, R.C., Owens, E.H., Sergy, G.A., 2002. Weathering of an Arctic oil spill over 20 years: the BIOS experiment revisited. Mar. Pollut. Bull. 44 (11), 1236–1242.
Prouty, N.G., et al., 2016. Impact of Deepwater horizon spill on food supply to deep-sea benthos communities. Estuar. Coast. Shelf Sci. 169, 248–264.
Quigg, A., et al., 2019. Marine Oil Snow Sedimentation and Flocculent Accumulation (MOSSFA) events: learning from the past to predict the future. In: Deep Oil Spills: Facts, Fate and Effects, first edition. Springer International Publishing, Switzerland, VIII, pp. 612.
Romero, I., et al., 2015. Hydrocarbons in Deep-Sea sediments following the 2010 Deepwater Horizon Blowout in the Northeast Gulf of Mexico. PLoS One 10 (5), e0128371.
Romero, I., et al., 2017. Large-scale deposition of weathered oil in the Gulf of Mexico following a deep-water oil spill. Environ. Pollut. 228, 179–189.
Schwing, P.T., et al., 2017. Constraining the spatial extent of marine oil snow sedimentation and flocculent accumulation following the Deepwater horizon event using an excess 210Pb flux approach. Environ. Sci. Technol. 51 (11), 5962–5968.
Schwing, P.T., O'Malley, B.J., Hollander, D.J., 2018. Resilience of benthic foraminifera in the northern Gulf of Mexico following the Deepwater Horizon event (2011–2015). Ecol. Indic. 84, 753–764.
Setti, L., Lanzarini, G., Pifferi, P.G., Spagna, G., 1993. Further research into aerobic degradation of n-alkanes in a heavy oil by a pure culture of Pseudomonas spp. Chemosphere 26, 1151–1157.
Shipe, R.F., Brzezinski, M.A., 2001. A time series study of silica production and flux in an eastern boundary region: Santa Barbara Basin, California. Glob. Biogeochem. Cycles 15 (2), 517–523.
Simoneit, B.R.T., 1986. Cyclic terpenoids of the geosphere. In: Biological Markers in teh Sedimentary Record. Amsterdam, Elsevier.
Smetacek, V.S., 1985. Role of sinking in diatom life-history cycles: ecological, evolutionary, and geological significance. Mar. Biol. 84, 239–251.
Socolofsky, S.A., Adams, E.E., Sherwood, C.R., 2011. Formation dynamics of subsurface hydrocarbon intrusions following the Deepwater Horizon blowout. Geophys. Res. Lett. 38, L09602.
Spier, C., Stringfellow, W.T., Hazen, T.C., Conrad, M., 2013. Distribution of hydrocarbons released during the 2010 MC252 oil spill in deep offshore waters. Environ. Pollut. 173, 224–230.
Stout, S.A., German, C.R., 2018. Characterization and Flux of Marine Oil Snow Settling toward the Seafloor in the Northern Gulf of Mexico during the Deepwater Horizon Incident: Evidence for Input from Surface Oil and Impact on Shallow Shelf Sediments. Mar. Pollut. Bull. 129 (2), 695–713.
Stout, S.A., Payne, J.R., 2016a. Macondo oil in deep-sea sediments: part 1 – sub-sea weathering of oil deposited on the seafloor. Mar. Pollut. Bull. 111 (1–2), 365–380.
Stout, S.A., Payne, J.R., 2016b. Chemical composition of floating and sunken in-situ burn residues from the Deepwater horizon oil spill. Mar. Pollut. Bull. 108 (1–2), 186–202.
Stout, S.A., Payne, J.R., 2017. Footprint, weathering, and persistence of synthetic-base drilling mud olefins in deep-sea sediments following the Deepwater Horizon disaster. Mar. Pollut. Bull. 118, 328–340.
Stout, S.A., Payne, J.R., Ricker, R.W., Baker, G., Lewis, C., 2016a. Macondo oil in deep-sea sediments: part 2 — distribution and distinction from background and natural oil seeps. Mar. Pollut. Bull. 111 (1–2), 381–401.
Stout, S.A., Payne, J.R., Emsbo-Mattingly, S.D., Baker, G., 2016b. Weathering of field-collected floating and stranded Macondo oils during and shortly after the Deepwater horizon oil spill. Mar. Pollut. Bull. 105 (1), 7–22.
Stout, S.A., Rouhani, S., Liu, B., Oehrig, J., Ricker, R.W., Baker, G., Lewise, C., 2017. Assessing the footprint and volume of oil deposited in deep-sea sediments following the Deepwater Horizon oil spill. Mar. Pollut. Bull. 114, 327–342.
Utermöhl, H., 1958. Zur Vervollkommnung der quantitativen Phytoplanktonmethodik. Internationale Vereinigung für Theoretische und Angewandte Limnologie, Mitteilungen 9, 1–38.
Valentine, D.L., et al., 2014. Fallout plume of submerged oil from Deepwater horizon. Proc. Natl. Acad. Sci. 111 (45), 15906–15911.
Venkatesan, M.I., 1988. Occurrence and possible sources of Perylene in marine sediments - a review. Mar. Chem. 25, 1–27.
Wang, Z., et al., 1999. Quantitative characterization of PAHs in burn residue and soot samples and differentiation of pyrogenic PAHs from Petrogenic PAHs - the 1994 Mobile burn study. Environ. Sci. Technol. 33, 3100–3109.
Wang, Z., Fingas, M., Owens, E.H., Sigouin, L., Brown, C.E., 2001. Long-term fate and persistence of the spilled Metula oil in a marine salt marsh environment degradation of petroleum biomarkers. J. Chromatogr. A 926, 275–290.
White, H.K., et al., 2012. Impact of the Deepwater horizon oil spill on a deep-water coral community in the Gulf of Mexico. Proc. Natl. Acad. Sci. 109 (50), 20303–20308.
Wirth, M., Passow, U., Jeschek, J., Hand, I., Schulz-Bull, D.E., 2018. Partitioning of oil compounds into marine oil snow: insights into prevailing mechanisms and dispersant effects. Mar. Chem. 206, 62–73.
Yan, B., et al., 2016. Sustained deposition of contaminants from the Deepwater Horizon spill. PNAS 113 (24), E3332–E3340.
Ziervogel, K., et al., 2012. Microbial activities and dissolved organic matter dynamics in oil-contaminated surface seawater from the Deepwater horizon oil spill site. PLoS One 7 (4).